

A MULTIDIMENSIONAL STUDY OF KINEMATICS AND EXCITATION OF
MOLECULAR GAS IN PLANET-FORMING REGIONS

by

José Ángel Pérez Chávez, B.S.

A thesis submitted to the Graduate Council of
Texas State University in partial fulfillment
of the requirements for the degree of
Master of Science
with a Major in Physics
August 2022

Committee Members:

Andrea Banzatti, Chair

Blagoy Rangelov

Aditya Togi

COPYRIGHT

by

José Ángel Pérez Chávez

2022

FAIR USE AND AUTHOR'S PERMISSION STATEMENT

Fair Use

This work is protected by the Copyright Laws of the United States (Public Law 94-553, section 107). Consistent with fair use as defined in the Copyright Laws, brief quotations from this material are allowed with proper acknowledgement. Use of this material for financial gain without the author's express written permission is not allowed.

Duplication Permission

As the copyright holder of this work I, José Ángel Pérez Chávez, authorize duplication of this work, in whole or in part, for educational or scholarly purposes only.

DEDICATION

Este trabajo está dedicado a todos los que me apoyaron a lo largo de mi carrera de pregrado y maestría. A viejos amigos que se mantuvieron en contacto, y a nuevos amigos con los que he pasado incontables horas trabajando. A amigos de mi Grupo Folklorico Ocotochtli y al tiempo que pasamos bailando y divirtiéndonos. A mi familia que están en México y no pueden estar presentes, pero siempre los tengo en mi mente. A mis tres hermanas Lilia, Janeth, Lizeth y mis seis sobrinos David, Aristeo, Leonardo, Enrique, Estrella y Sakura quienes amo mucho y los guardo en mi corazón todos los días. Y por último a mi mamá Rosa María Perez Chavez, a quien más amo y quien siempre me apoyó en todos los sentidos para continuar mi educación y siempre creyó en mí.

This work is dedicated to everyone who supported me throughout my undergraduate and master's career. To old friends who stayed in contact and reached out from time to time, and new friends who I've spent countless hours working with. To my friends in the Grupo Folklorico Ocotochtli and the time we spent dancing and having fun together. To my family who are in Mexico and cannot be present, but I always keep them in mind. To my three sisters Lilia, Janeth, and Lizeth and my six nephews David, Aristeo, Leonardo, Enrique, Estrella, and Sakura who I love dearly and keep them in my heart every day. Lastly, to my mom Rosa María Perez Chavez who I love the most, who always supported me in all ways to continue my education and always believed in me.

ACKNOWLEDGEMENTS

I would like to express my gratitude and appreciation to my advisor, mentor, and chair committee member Dr. Andrea Banzatti. His guidance and support were key in the completion of this project and my professional development. Thanks to my other committee members Dr. Rangelov and Dr. Togi for being part of the final stages of the project and being understanding throughout the process. Thanks to the rest of our protoplanetary disk research group who provided feedback to my work multiple times.

TABLE OF CONTENTS

	Page
ACKNOWLEDGEMENTS.....	v
LIST OF TABLES.....	vii
LIST OF FIGURES.....	viii
LIST OF ABBREVIATIONS.....	ix
ABSTRACT.....	xi
 CHAPTER	
I. INTRODUCTION.....	1
Young Stellar Objects.....	1
Protoplanetary Disks & The Inner Planet Forming Regions.....	3
CO Rovibrational Emission.....	5
Fundamental Emission Lines: Keplerian vs Winds.....	6
Sample & Data.....	8
II. METHODS.....	12
III. RESULTS AND DISCUSSION.....	17
CO Luminosity: Thick Inner Rim & Dusty Winds.....	17
R_{CO} , Sublimation Radius vs Stellar Luminosity.....	21
Revisiting The Inner Rim R_{CO} & R_{sub} Correlation.....	23
Discussion of Keplerian Emitting Regions.....	26
Molecular Wind in Transitional Disks.....	30
Low Mass Disks.....	32
Outliers.....	32
IV. CONCLUSION.....	34
APPENDIX.....	38
REFERENCES.....	44

LIST OF TABLES

Table	Page
1. Median and HDI for the slope, correlation coefficient, and intrinsic scatter for each the linear regression fits of CO luminosity.....	21
2. Median and HDI for the slope, correlation coefficient, and intrinsic scatter for each the linear regression fits of CO emitting radii.....	23

LIST OF FIGURES

Figure	Page
1. Overview of the protostar and pre-main sequence (PMS) stages with their respective measured SEDs	3
2. Modified illustration from Banzatti et al. (2022) of the representatives line shapes for the two identified kinematics.....	6
3. Stellar and disk properties of the 51 protoplanetary disks in our sample	9
4. Empirical dust sublimation radius and infrared index vs Stellar mass	11
5. CO luminosity (broad/single component) as a function of stellar mass (left) and luminosity (right)	17
6. CO Luminosity as a function of inclination.....	18
7. Interpretation of BC and NC in triangular lines within the context of a multi-shell wind launched near the dust sublimation radius.....	20
8. CO characteristic emitting radius (broad/single component) measured from the HWHM as a function of stellar luminosity.	22
9. CO characteristic emitting radii normalized by the empirical radii vs total luminosity.	23
10. CO emitting radii measured from the width of emission line base (10%) that traces the fastest CO and closest to the star.	25
11. CO emitting radii of innermost CO normalized by the empirical sublimation radii of each system vs the total luminosity	26
12. Schematic of three main Keplerian emission regions.....	26
13. CO luminosity (BC/SC) as a function of CO characteristic emitting radii	30
14. Schematic of molecular winds within dust depletion regions	30

LIST OF ABBREVIATIONS

Abbreviation	Description
AU	Astronomical Unit
Myr	Million years
PMS	Pre-main sequence
SED	Spectral Energy Distribution
TTs	T-Tauri stars
HAeBe	Herbig Ae/Be stars
VLT	Very Large Telescope
IRTF	Infrared Telescope Facility
CRIRES	CRyogenic InfraRed Echelle Spectrograph
CO	Carbon Monoxide
BC	Broad Component
NC	Narrow Component
SC	Single Component
n_{13-30}	Spectral infrared index between 13 and 30 μm
FWHM	Full Width at Half Maximum
FW10%	Full Width at 10% or zero intensity
μm	Micrometer, or micron (10^{-6} meters)
Jy	Jansky (unit of flux density)
IR	Infrared

ETI	Equal-Tailed Interval
HDI	Highest Density Interval
MCW	Magnetocentrifugal winds
MRI	Magnetorotational instability

ABSTRACT

Protoplanetary disks are rotating gas and dust around young, pre main sequence stars and are predecessors to planetary systems like our solar system. The fundamental rovibrational emission band of CO at 4.7 μm is a key diagnostic of the structure of the warm inner 10 AU and planet-forming regions in these disks. By observing CO at high spectral resolution, we distinguish double peak and triangular shaped emission lines that trace Keplerian disk rotation and an additional slow wind component, respectively. To better understand the dichotomy between these lines and the structure of inner disks we employ a multidimensional study on a sample of 51 protoplanetary disks from two high resolution spectroscopy surveys using VLT-CRIRES and IRTF-iSHELL. We studied CO emission excitation and emitting regions with conjunction of star/disk properties including stellar mass, disk inclination, accretion luminosity, and infrared index that traces inner disk cavities. We find three main emitting regions of Keplerian emission based on the host stellar masses: gas within cavities for 1.5-2 M_{\odot} , gas on a surface layer for 1.7-3.6 M_{\odot} , gas at the inner rim of the disk for 3.5-5.2 M_{\odot} . For wind emission we find an interesting case of molecular winds emitting at 0.5-35 AU from the stars, well inside large cavities of up to 70 AU. We discuss the excitation environments, emitting regions, and structures of these cases to improve our understanding of CO molecular gas emission in these planet-forming regions.

I. INTRODUCTION

The origin of life is one of the biggest mysteries of humanity. It requires the input from many different fields in science, and astronomy is a key one among them. The formation of a star and planet-forming circumstellar material is one of the biggest fields within astronomy that connects to the origins of life. These systems undergo mutual interactions between the star and the surrounding disks and eventually form planets that orbit the star. As the disk evolves, material accretes to the star and the planet, and this includes the delivery of organics associated to life. These young systems set the initial conditions for the potential of life in the future of their planets. Super-Earths and terrestrial planets are considered to form in the inner regions of these disks. Thus, disk structure and evolution can play an important role in the formation and composition of planets (Armitage 2010). During planet formation, the mass of the protoplanetary disk is dominated by gas, and the gas-to-dust mass ratio is close to 100:1. The structure and kinematics of inner disks are therefore strongly determined by protoplanetary gas. In this thesis, I investigate the inner regions of protoplanetary disks and examine the structure and kinematics of molecular gas emission, to better understand their physical structure.

Young Stellar Objects

Stars are formed from the interstellar medium and their formation begins with the collapse of a cold dense molecular cloud. Cloud cores collapse onto a rotating disk through conservation of angular momentum and accrete mass to a young protostar at the center. The disk rotation and accretion produce turbulent viscosity, stellar jets and outflows, and disk winds which clear up the surrounding remnant envelope leaving behind a star and disk system, until the disk itself disperses away. Young stellar objects

(YSO) with infrared excess indicative of circumstellar disks are broadly classified into different classes based on their spectral energy distribution (SED, see Figure 1 for an overview). In Class 0, the central protostar is embedded and completely obscured by the surrounding material and the envelope dominates the spectral energy distribution at long wavelengths. In Class I, the protostar is visible in the SED but the large infrared excess due to the clearing envelope still dominates and is forming a disk-like structure. In Class II, the stellar black body and the disk can finally be distinguished in the SED and nearly all the envelope of material has cleared with exception of a flat circumstellar disk with ongoing planet formation. At this stage the star is considered pre-main sequence as it has acquired most of its mass but has not yet started nuclear fusion. Class II or protoplanetary disks are the longest-lived stage with a lifetime of several Myr and the interactions between star and disks set some stellar and planetary properties that persist for billions of years. Finally, in Class III systems most of the disk has been dispersed through dust evolution, wind clearing, and planet formation, leaving little or no IR excess in the SED. These classes are thought to be different stages of early planetary system evolution.

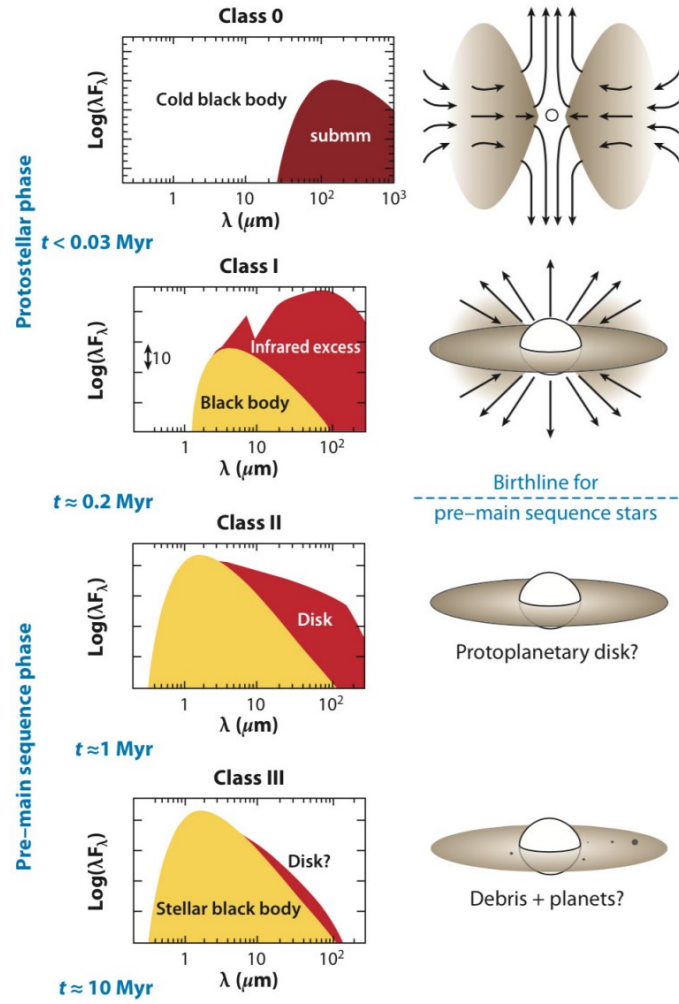


Figure 1. Overview of the protostar and pre-main sequence (PMS) stages with their respective measured SEDs.

Protoplanetary Disks & The Inner Planet Forming Regions

Class II protoplanetary systems can further be labeled or classified into systems that describe their stellar and observational properties. Pre-main sequence (PMS) stars are classified as Herbig Ae/Be (HAeBe) or T-Tauri (TTs/cTTs) stars. T-Tauri stars comprise young stars of mass lower than $1.5 M_{\odot}$; they have long been known to be variable at UV, optical and infrared wavelengths in connection to variable accretion from their circumstellar disk. HAeBe are the higher mass analogs to TTs with a range of $2 - 8 M_{\odot}$. When disks around HAeBe or TTs form an inner dust cavity, sometimes as large as 100

AU, they are called “transitional” (Espaillat et al., 2014). The label “transitional” comes from the idea that these cavities indicate dispersal and an evolution phase towards a Class III system where most of the disk is gone.

The inner regions of these systems consist of warm and hot gas and dust, where the innermost gas accretes onto the star. This dust and gas emit in the near and mid infrared part of the spectrum due to the high temperature (up to a few 1000 K). Dust becomes optically thick at optical and IR wavelengths and dominates the SED of these systems. Hence, we can only observe molecular gas above or within the optically thick layers of dust. These systems have optically thick midplanes, and optically thin surface layers that extend to the inner rim of the disks. These regions allow emission from molecular gas to escape the dust and reach us.

IR spectroscopy is the leading technique to observe warm and hot molecular gas emission in protoplanetary disks at < 10 AU from the central star. Two decades ago, the Spitzer Space Telescope offered unmatched sensitivity and spectral coverage of multiple molecules at 10 – 35 microns and initiated the very first comprehensive surveys of the molecular content in the inner regions of protoplanetary disks. The development of high-resolution spectrographs opened a new phase to study disk rotation, gas outflows, and asymmetries or variability in gas distributions through the observed spectral line broadening. The Near Infrared Spectrograph on the Keck telescopes (Keck-NIRSPEC; $R \sim 25,000$), CRyogenic InfraRed Echelle Spectrograph on the Very Large Telescope (VLT-CRILES; $R \sim 94,000$), and now iSHELL instrument on the Infrared Telescope Facility (IRTF-iSHELL $\sim 60,000$ - $92,000$) have provided high resolving power and resolved the kinematics of gas emission, covering narrow spectral ranges typically

centered on CO emission around 4.7 μm .

CO Rovibrational Emission

The fundamental rovibrational band (i.e., rotational transitions between different vibrational states) of CO at 4.4-5.3 μm is a key diagnostic of the structure of planet-forming regions. It is particularly sensitive to warm/hot temperatures in the inner disk (300-2000 K), 0.1 – 10 AU, and the low opacity at high altitudes in the disk molecular layer. Rovibrational CO emission is present throughout a wide range of protoplanetary disks (Najita 2003; Brittain 2007; Salyk 2009; Pontoppidan 2011; Brown 2013). CO has been observed over a large range of gas temperatures ($\sim 100 - 3000$ K), it requires relatively small column densities to produce bright lines that we can observe, and it is expected to survive even in regions where there is little dust shielding from UV photodissociation. Relatively high Einstein A-coefficients, low excitation temperature of fundamental CO transitions, together with the resistance of the CO molecule to thermal and photo-dissociation make CO gas an ideal tracer of molecular gas in these regions. The CO lines have been used to determine excitation mechanisms (IR/UV pumping & collisional excitation), depletion of gas/dust in the inner disk, and trace winds and outflows from the disk surface.

Fundamental Emission Lines: Keplerian vs Winds

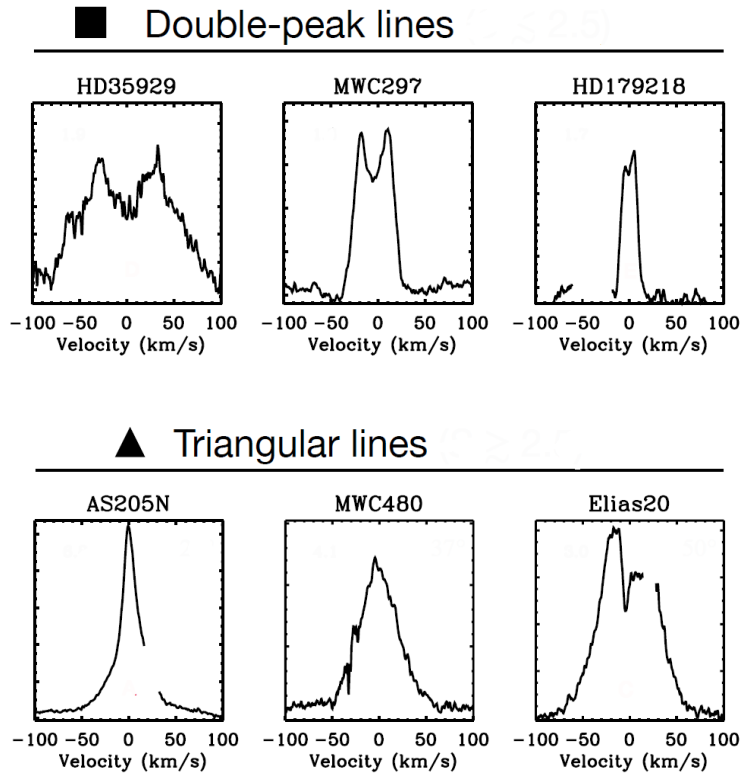


Figure 2. Modified illustration from Banzatti et al. (2022) of the representative line shapes for the two identified kinematics. Top row are double peaked lines that trace Keplerian rotating rings of gas, and bottom row are triangular lines.

Two fundamental types of CO line profiles have been identified and studied so far as seen in Figure 2. Double peak emission profiles are associated with disk rings in Keplerian motion and Keplerian models fit the profiles very well. These profiles are commonly found in disks around H AeBe stars. A distinct type of line profile, instead, can be identified by a triangular shape that has steeper line wings and a single line peak at the line center, that in the broadest lines is usually observed to be asymmetric and variable. Triangular line profiles are less understood but are commonly attributed to disk emission with a slow molecular gas winds due to the common narrow peaks, asymmetries, and line shifts towards the blue. Triangular lines are commonly found in disks around TT stars.

These lines are commonly decomposed into broad and narrow components (BC/NC) that consist of the line wings and the line center respectively, which show different kinematic and excitation properties with the broad component being more vibrationally excited than the narrow (Banzatti & Pontoppidan, 2015). The advantage over single component (SC) emission analysis is that different emission regions can be distinguished from the BC and NC. The NCs cannot readily be explained by just Keplerian motions of gas in the inner disk. These types of lines have been discussed in previous work and described by comparing the line peak width and the base width (Banzatti et al., 2022; Bast et al., 2011)

Bast et al. (2011) uses CRIRES high resolution spectra to explore a small subsample of 8 disks with these narrow lines. They find these disks are accreting onto their central stars at high rates relative to the parent sample, and the lines are excited, at least in part, by UV-fluorescence. They conclude the most likely interpretation is a slow-moving disk wind, launched by either EUV emission or soft X-rays.

Banzatti et al. (2022) measured the shape parameter for two CO surveys using CRIRES and iSHELL. They further reinforce the idea that a slow disk wind component produces narrow peak lines but adds that broader base lines may be produced due to the Keplerian disk. They further add that differences in wing sizes are due to different inclination views. These complexities lead to a closer global view of line types.

In this work we study CO line emission shapes in context of the molecular excitation, and star/disk properties. Our sample of 51 protoplanetary disks of a wide range of properties from two different surveys using VLT-CRIRES and IRTF-iSHELL. Our analysis focuses on the line emission spectra products for $^{12}\text{CO } v = 1-0$; and star/disk properties including stellar mass/luminosity, effective temperature, accretion luminosity,

and infrared excess that traces inner cavities. We applied correlation analyses to triangular and double peaked CO lines separately and diagnose the multiple trends and properties that differentiate CO emission in Keplerian disk rings vs disk winds. This type of multidimensional study is only possible with comprehensive samples, and tools that guide our understanding of the complexity of trends in the data. Our analysis will build on previous empirical works and highlight the importance of CO emission line shapes in improving our understanding of the structure and evolution of planet forming regions.

Sample & Data

The sample analyzed in this work includes 51 protoplanetary disks around pre-main sequence stars of a wide range of properties. The sample include CTTS, HAeBe systems, and transitional disks. The systems span a large range of spectral types A5 – K5 with temperatures from $\sim 1500\text{K}$ to $14,000\text{K}$, stellar masses of $0.4 - 20M_{\odot}$, and luminosities of up to $800 L_{\odot}$. In addition, the sample includes distances up to 900 pc, and disk inclinations that roughly span the whole 90 degrees. The distributions of some of these parameters can be seen in Figure 3. Accretion luminosity measurements are taken from Salyk et al (2013), Fang et al (2018), Wichittanakom et al. (2020), Guzman-Diaz et al (2021) for roughly $\sim 50\%$ of the sample and the rest from other works listed under Table B1.

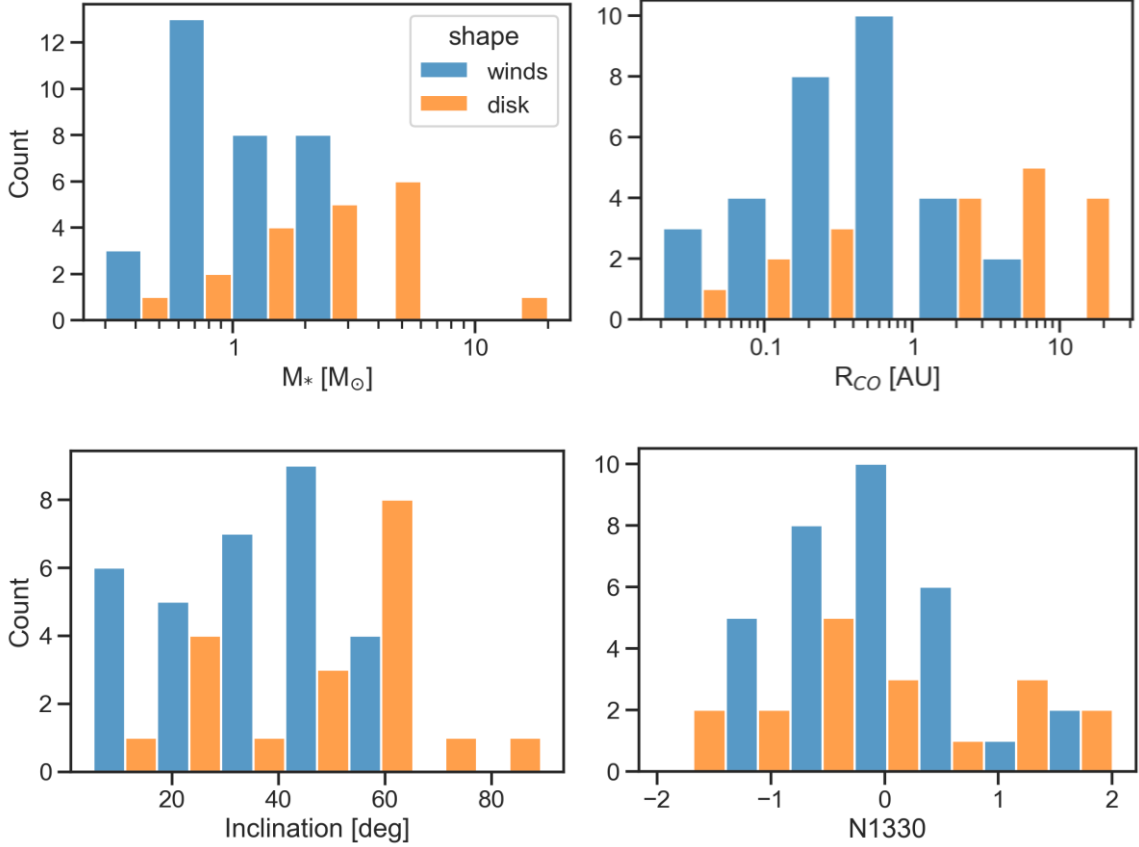


Figure 3. Stellar and disk properties of the 51 protoplanetary disks in our sample. R_{CO} for wind emission is calculated from the BC, more about this in the methods section.

The infrared index n_{13-30} is crucial in our dataset of diverse inner dust depletions, originally studied by Furlan et al (2006, 2009). The 13/30 μm SED spectral slope is a measure of the degree of grain settling in the disk atmosphere and traces inner disk dust cavities (Brown et al., 2007; Furlan et al., 2011). It is measured as in Banzatti et al. (2019) from narrow spectral ranges that avoid molecular emission at 13.31 μm and 30.1 μm , and characterized by

$$n_{13-30} = \frac{\log(\lambda_{30}F_{\lambda_{30}}) - \log(\lambda_{13}F_{\lambda_{13}})}{\log(\lambda_{30}) - \log(\lambda_{13})}.$$

where values larger than ~ 0 trace dust depletion and inner cavities, and values < 0

trace disks with fuller dust inner regions. An overview of the distribution of values in our sample is found in Figure 3.

The molecular spectra analyzed in this work were taken with VLT-CRIRES and IRTF-iSHELL as part of separate and complementary surveys of M-band CO spectra from protoplanetary disks. In this work I focus on the extracted stacked line fluxes of $^{12}\text{CO } \nu=1-0$. The spectra products are composed of line fluxes, central line wavelengths, and line widths. The line widths are especially useful as they represent the kinematic information of the disks and can be used to calculate the radial location of the CO gas, which is discussed in the next section.

Dust sublimation sets the stellar distance at which the dusty disk begins, i.e. the inner edge or inner wall of the dusty disk; inside of this radius and closer to the star temperatures are too hot and even dust sublimates into gas and is eventually accreted onto the star. In order to compare the location of CO to the sublimation radius of each system I include empirical dust sublimation measurements from Banzatti et al. (2022). These empirical dust radii measurements are extrapolated from a moving mean on dust near-infrared interferometry measurements from Marcos-Arenal et al. 2021. The distribution of sublimation radii in our sample is shown in Figure 4.

Details on the data reduction and extraction procedures can be found in the original references listed above. To calibrate these continuum-normalized line fluxes I use W2 fluxes from WISE and taken from the AllWISE Data Release (Cutri et al. 2021).

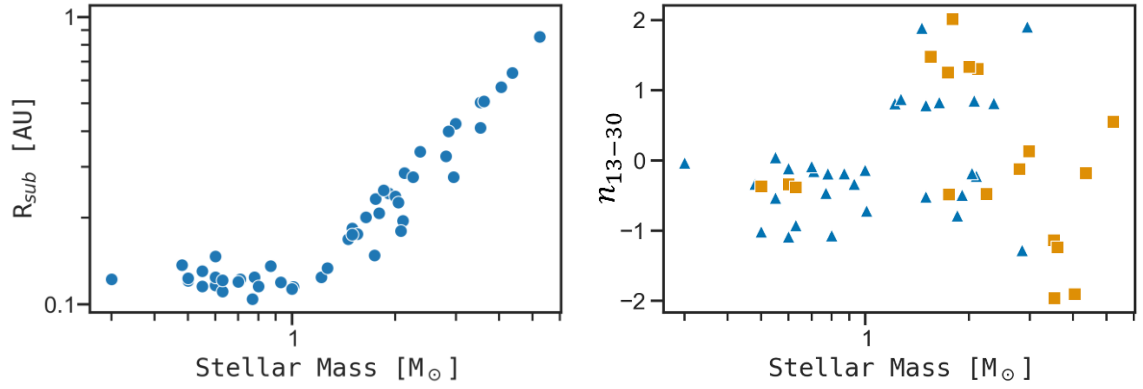


Figure 4. Empirical dust sublimation radius and infrared index vs Stellar mass. Blue triangles are disks with wind emission, and orange squares are disks with Keplerian emission. These illustrate the distribution of disk parameters across the stellar masses of our sample. The sublimation radius is correlated to the stellar mass as expected as the radius moves outward for hotter and brighter stars.

II. METHODS

Investigating processes that affect the measured CO line luminosities, the gas location and kinematics is intrinsically a multidimensional problem. NIR molecular spectra are expected to strongly depend on gas heating and cooling, and their dependence on the inner disk irradiation, geometry, dust/gas density and their vertical/radial distributions, among other factors. Molecular luminosities correlate with stellar luminosity, and accretion luminosity supporting a strong role for gas heating processes. At the same time, we expect massive stars to easily photo dissociate molecular gas near the star, and push both molecular and dust emission farther out. Molecular luminosities decrease when inner disk cavities form, suggesting that inner disk molecular gas gets depleted when dust is depleted. Geometrical properties like inclination present another challenge. We expect low and high inclination systems to be more sensitive to different emitting regions for example the high inclination systems could reveal the inner rim wall of the inner disk better than low inclined systems. In addition, inner disk cavities can be “hidden” in highly inclined systems, and present correlations between inclination and infrared index. To tackle these multiple correlations, it is necessary that we analyze the parameter grid and be mindful of the intrinsic scatter each variable presents due the multiple dependencies between one another. While we don’t need to understand the origin of these dependencies and scatter, we can build tools and a procedure to take the intrinsic scatter and other uncertainties into account.

Common procedures adopted in other works, correlations are assessed with both Pearson’s correlation test for linear relations and Spearman’s rank correlation test for monotonic relations. However, as in Hendler et al. (2020), we remark that both these tests

have their limitations in capturing correlations, one being the fact they cannot account for measurement errors and upper limits. Therefore, to better assess correlations we adopt the probability-based linear regression method by Kelly (2007) which accounts for upper limits and measured uncertainties. Pascucci et al. (2016) used this method to determine a steep linear relation between millimeter flux and stellar mass in Chamaeleon I that accounts for censored data (e.g., upper limits), and measurement errors. This complex method is suited for multidimensional analysis as it also characterizes an intrinsic scatter about the regression line due to other unknown physical properties.

Therefore, this method attempts to extract an underlying linear relationship that is obscured in multivariate measurements. The details in the model can be found in Kelly 2007. For the purposes of assessing the underlying relationships across stellar and disk properties, we focus on the regression parameter slope β , standard deviation of intrinsic scatter σ , and correlation coefficient ρ from the estimated posterior distribution of the statistical model. For example, we can fit CO line luminosity measurements vs host star masses, and visually assess the best-fit line and estimated parameters. The posterior distributions are defined by random draws for each regression parameter from the model. We can calculate the median and confidence interval of each parameter and plot the median regression line as defined by the model without the scatter, $y = \alpha + \beta x$ where α is a regression parameter as well, to assess the quality of the estimated relationships. To calculate a confidence interval that summarizes each regression parameter, I opt to use the Highest Density Interval (HDI). This interval includes the most credible values in the probability density distribution, and works great in skewed distributions, and behaves like an equal-tailed interval (ETI) of 90-97% percentile in symmetric distributions (Kruschke

2015).

To analyze the multi-dimensionality of molecular emission in disks I designed a tool for complex datasets that applies the correlation method mentioned above. The program designs a grid of scatter plots for all parameters in the dataset in linear or logarithmic space and fit a Bayesian-based linear regression model based on Kelly (2007) method. The program uses the package seaborn as foundation and other libraries as matplotlib, astropy, numpy, and scipy. As an initial testing run, I applied the correlation grid to mid-infrared spectra taken in a new survey with VLT-VISIR that detects H₂O and Ne II lines. It provided an opportunity to explore the expected effects of disk inclination and inner gas/dust depletion effects in line emission widths. Now, this tool provides large overviews of our line emission and system properties, and correlations among them. This help us explore different properties in parallel and determine what correlations are worth looking into. The starting properties include those in the dataset with special focus on CO luminosities, stellar mass and luminosity, effective temperature, accretion luminosity, infrared index, and inclination. Total luminosity is the composition of the stellar and the accretion luminosity to represent the total central luminosity that the inner disk is exposed to.

The CO luminosity (L_{CO}) is calculated using the line fluxes in conjunction of the distance measurements and AllWise 4.6-micron continuum fluxes. The emission line Half Width at Half Maximum (HWHM) can be used to calculate a characteristic CO radius, R_{CO} . While one could extract a CO radial profile using a Keplerian model from the line, this is time-consuming. Instead, the HWHM provides an estimate of the radial CO emission peak location for a Keplerian profile. Banzatti et al. (2022) shows this

estimate does well at defining a position where most of the emission is located, compared to a complete Keplerian profile model fit. The line HWHM measurement is converted from wavelength to velocity using a modified doppler shift equation,

$$v = c \frac{\Delta\lambda}{\lambda_c}$$

where λ_c is the central wavelength of the emission line, $\Delta\lambda$ is the line width, c is the speed of light, and v is the calculated velocity. Under Keplerian motion this velocity measurement can be used to calculate the gas distance from the star using

$$R_{CO} = \frac{GM \sin^2 i}{v^2}. \quad 1$$

This calculation requires the stellar mass and inclination measurements for the system – all included in our dataset. The dominant uncertainty is from the inclination measurements, with increasing uncertainty for low inclination disks. A similar process can be done with the Full Width defined by the outer 10% percentile of the line (FW10%) of the line. This measurement instead provides us an estimate of the fastest moving gas in the CO ring that causes the Keplerian broadening or in other words the CO inner radius.

The radial location of CO in the triangular emission like systems is largely uncertain and not understood. Similar to the Keplerian emission lines, the spatial location of the CO for triangular emission is calculated assuming Keplerian motion on the broad components or line wings. This is one of the advantages of component separation of CO emission lines, a narrow and broad component are separated to distinguish two different emitting regions or mechanisms. Banzatti et al (2022) showed the FWHM of triangular emission lines increases with disk inclinations, similar to what we expect and observe in Keplerian emission lines. A possible interpretation of the broad component of the

triangular lines is that it represents the wind launching region within the system, which is likely more Keplerian than the narrow component, and therefore serves as an approximation. The narrow component – wind component – is far from Keplerian and we cannot estimate the radial location of its emitting region.

III. RESULTS AND DISCUSSION

During the vetting of spectral and protoplanetary parameters for the full grids of correlations we learned that stellar mass, total luminosity, inclination, infrared index, CO emitting radius, and CO luminosity are all important factors to compare and analyze. A full grid of relevant parameters with linear regression fits can be found in the Appendix. In the analysis discussed in this work, we focus on a subset of significant correlations.

CO Luminosity: Thick Inner Rim & Dusty Winds

The first significant correlation we found in our grid was CO luminosity vs stellar mass. L_{CO} in Keplerian-type spectra is tightly correlated with stellar mass, as opposed to CO in wind-type spectra that shows a large scatter and no obvious trend. This trend is found with the stellar and accretion luminosities as expected, because these properties are related to each other. In Figure 5, we can see that L_{CO} for the Keplerian subset has strong

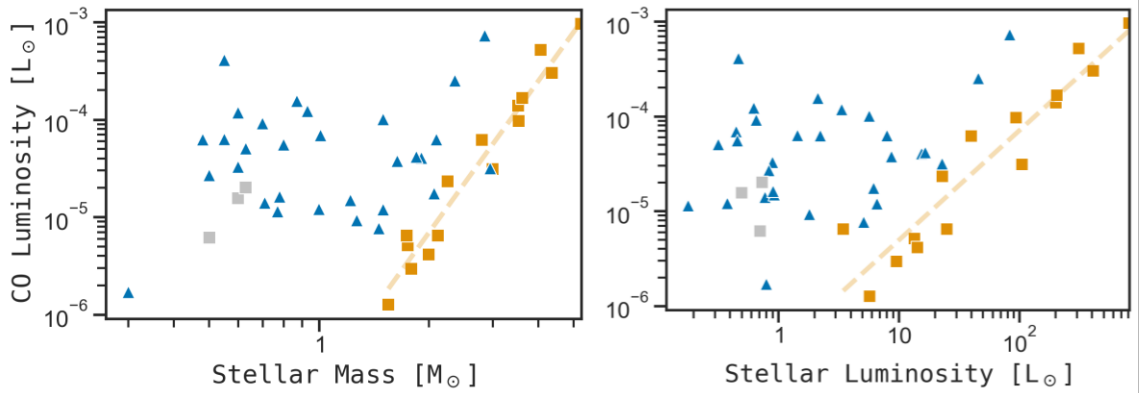


Figure 5. CO luminosity (broad/single component) as a function of stellar mass (left) and luminosity (right). Gray squares are low mass cTTs with Keplerian emission that we consider outliers in the analysis. The dashed orange line is the median best fit line of each Keplerian emission relation. The median stats and HDI of the regression parameters are included in Table 1.

correlations with stellar mass and luminosity as $L_{CO} \propto M_*^{5.2}$ and $L_{CO} \propto L_*^{1.15}$. CO luminosity increases almost one-to-one with respect to stellar luminosity. Keplerian-type spectra are more sensitive to changes in the stellar mass and therefore heating due to star,

than the wind-type. This could be understood considering that the Keplerian emission is physically on the disk itself, and the molecular gas should follow a thermal profile dictated by the star and disk dynamics. There are three low mass TTs (IQ Tau, WaOph6, AA Tau, the grey squares in Figure 5) for which we observe Keplerian CO emission and do not follow the trend we discuss above. Perhaps, this indicates it is a phenomenon exclusive for H AeBe stars and their high radiation pressure and temperature interactions; another possibility is that the line profile in these 3 systems is modified by obscuration, since all three have high disk inclinations. In the rest of the analysis, we exclude these three low mass systems from the sample of Keplerian-type spectra. Protoplanetary disk winds are less understood and the temperatures and velocities are dictated by the mechanisms for which they are lifted off the disk and blown away. Any correlation between the stellar mass and the CO wind excitation might be attenuated through those processes.

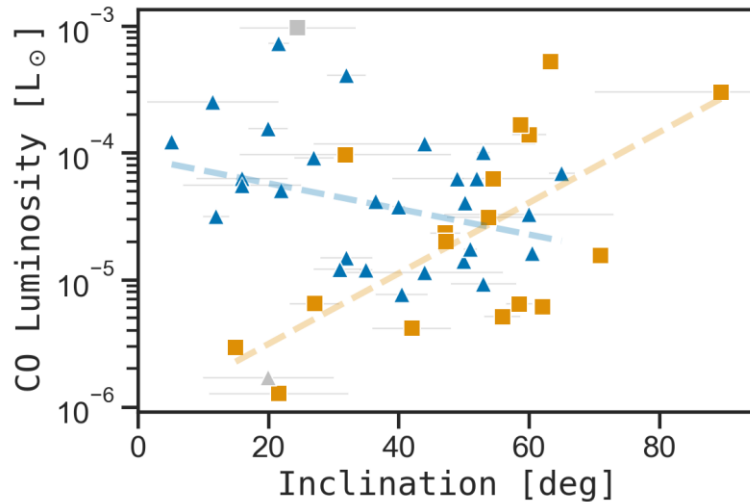


Figure 6. CO luminosity as a function of inclination. Legend is as in Figure 4 and 5. This time we don't exclude low mass cTTs with Keplerian emission. HD259431 and FN Tau are treated as outliers (gray squares) due to large deviations from the common trends. The line regressions suggest opposing trends for Keplerian and wind emissions.

A second significant correlation we noticed is the L_{CO} vs inclination shown in

Figure 6 In this analysis, we rejected two systems, HD259431 and FN Tau, due to the large deviations from the common trends. HD254931 is the the second most massive HAeBe star at $5.24 M_{\odot}$ with the highest L_{CO} and two CO rings. FN Tau is our cTTs with the lowest mass at $0.30 M_{\odot}$ and the lowest L_{CO} of single component narrow triangular emission. While the median regression line does not change drastically when the outliers are incorporated, we opted to exclude them to report and discuss the regression of parameters of the common trend. While the data show large scatter, different trends between the Keplerian and wind emission systems are well visible. The regression parameters have large confidence intervals (refer to Table 1) yet they do not overlap, supporting the different behaviours of the two kinematic populations. The different trends observed in the two populations seem to suggest geometrical effects can reveal or obscure part of the CO emitting area. Assuming a geometrically thick ring of gas in the disk, one can imagine the visible surface area of the inner wall to increase at larger inclinations, which would increase the measured L_{CO} . In this region, gas can potentially dominate in emission due to the higher temperatures. In fact, we observe the brightest CO in this region for massive stars. I discuss this result later in the Discussions section. A thick inner rim of CO can explain the increase in L_{CO} at larger inclinations for Keplerian emission, and the potential for the brightest CO to survive in this region further supports it. In the case of wind emission, we have a tentative shallow negative correlation between L_{CO} and inclination with smaller scatter than the Keplerian correlation. At larger inclinations, we expect dust+gas along line-of-sight to increase due to the disk wind and material extending across disk radii at high elevation or flaring. Observed narrow absorption components have been associated with this increase in gas column density

along high inclination due to the line of sight grazing the surface of the disk and crossing colder dusty winds (Andrea Banzatti et al., 2022). The dusty winds could obscure some of the dust-free wind emission in this scenario. Therefore, this possible decrease in CO brightness may be due to self-obscuration of the disk wind due to entrained dust within the wind.

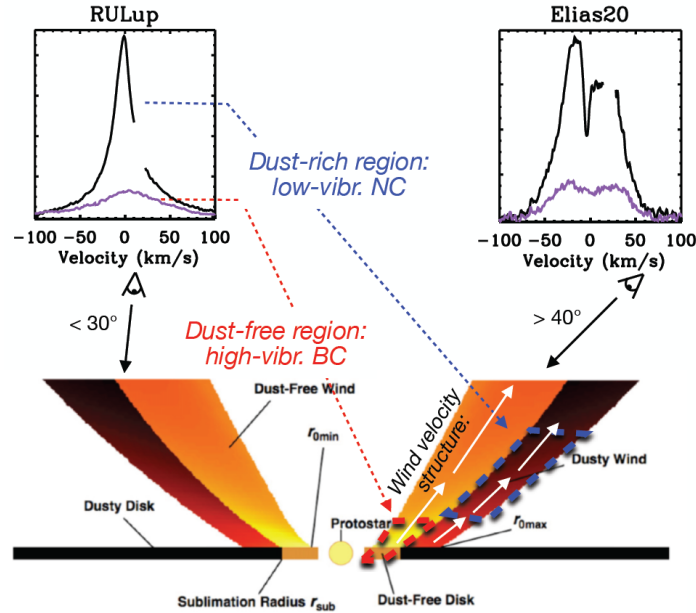


Figure 7. Interpretation of BC and NC in triangular lines within the context of a multi-shell wind launched near the dust sublimation radius. Taken from Banzatti et al. (2022). Note absorption from dusty colder wind and broadening happens at higher inclinations.

Another aspect to highlight is that the two disk populations overlap in the stellar and disk parameter space. The overlapping population of disks with host stars of $1.5-3 M_{\odot}$ and $1-50 L_{\odot}$ suggests wind CO emission is more luminous than double-peaked emission around similar host stars as seen in Figure 5. An additional factor in CO line intensities is the emission area, and since disk winds are known to be vertically extended regions, it is possible this factor increases the CO luminosity beyond the Keplerian emission for systems around similar host stars.

Table 1. Median and HDI for the slope, correlation coefficient, and intrinsic scatter for each the linear regression fits of CO luminosity.

Relation	Type	β - slope	ρ - corr. coeff	σ - scatter
L_{CO} vs M_*	Disk	$5.20^{+0.3}_{-0.4}$	$0.98^{+0.01}_{-0.02}$	$0.22^{+0.06}_{-0.05}$
L_{CO} vs L_*	Disk	$1.20^{+0.1}_{-0.2}$	$0.94^{+0.03}_{-0.05}$	$0.35^{+0.09}_{-0.07}$
L_{CO} vs $Incl.$	Wind	$-1.00^{+1.1}_{-1.2} \times 10^{-2}$	$-0.36^{+0.42}_{-0.36}$	$0.46^{+0.15}_{-0.12}$
	Disk	$2.77^{+2.2}_{-2.3} \times 10^{-2}$	$0.59^{+0.35}_{-0.43}$	$0.69^{+0.33}_{-0.24}$

R_{CO} , Sublimation Radius vs Stellar Luminosity

The emitting radius of CO (R_{CO}) is an important characteristic in this analysis as it provides crucial context of the location of the gas that we can use to determine the kind of environment the CO is exposed to. R_{CO} is estimated from the measured CO line widths using the stellar mass and disk inclination using Equation 1 . Figure 8 shows a positive correlation between R_{CO} of the combined population of emission types with stellar luminosity. This is reminiscent of the dust sublimation radius relation $R_{sub} \propto \sqrt{L_*}$ as seen in Eq. 2. While the scatter is large, the main take away is that smaller R_{CO} are found around colder stars, and larger radii are found around hotter stars, suggesting that CO gas moves to larger radii as a function of stellar luminosity (similarly to what's expected for the dust). Once we subdivide the data and separate wind launch emission from Keplerian emission, we can see they follow very separate trends (Figure 8, right panel). Similar to the CO Luminosity, this remarks how these two types of emission trace different behaviours within the protoplanetary disks in the sample. The wind launching emitting radii move to larger radii for hotter stars, similar to the overall trend and the dust sublimation radius, suggesting the CO in these systems moves out with the dust. For Keplerian emission we see the opposite trend. While these trend lines suggest a linear

relationship between these properties, we want to emphasize that this may not be the case but rather serve as a way to highlight different behaviours between wind and disk emission. The difference becomes more apparent once we normalize R_{CO} by R_{sub} in Figure 7. This ratio shows us how the CO emitting region moves relative to the sublimation radius and provides more context on the emitting environment. Once compared to R_{sub} , we see the wind emission radius changing more slowly and uncertain as a function of stellar luminosity, while the Keplerian emission downward trend becomes steeper. Therefore, this ratio becomes key when diagnosing the Keplerian emission regions. The statistics of the fitted linear regressions are found in the table below. These trends can be seen in the emitting inner radii of CO as well, and are discussed in the next section.

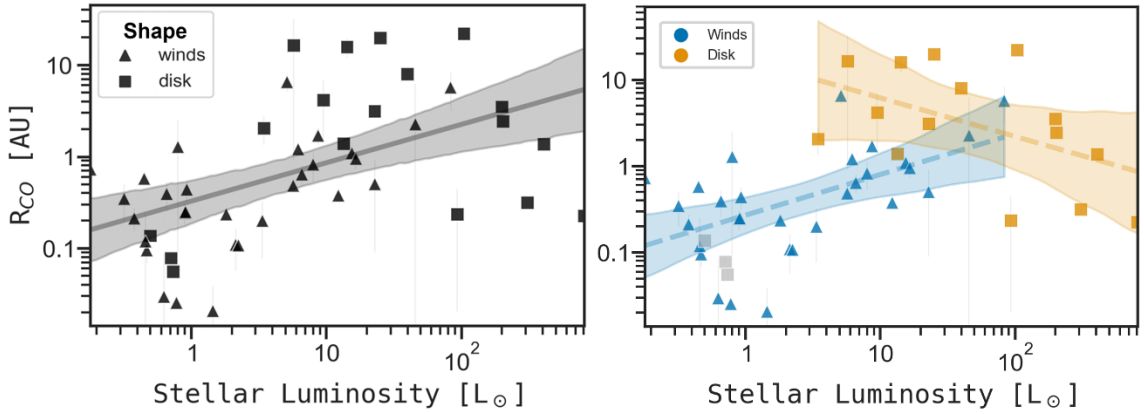


Figure 8. CO characteristic emitting radius (broad/single component) measured from the HWHM as a function of stellar luminosity. Gray squares on the right plot are low mass TTs with Keplerian emission that we consider outliers in the Keplerian analysis. The left panel shows all indistinguishable points fitted to highlight the general upward trend of the emitting radius, while points and the fit are colored by the kinematics on the right. Left:

$$\beta = 0.42_{0.23}^{0.62}, \rho = 0.54_{0.31}^{0.75}, \sigma = 0.63_{0.50}^{0.78}.$$

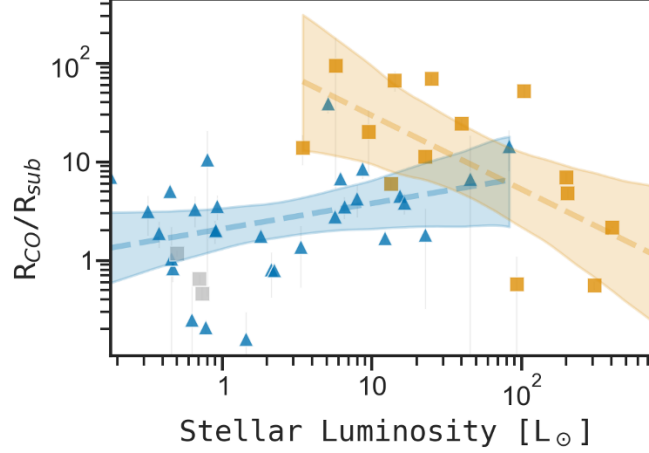


Figure 9. CO characteristic emitting radii normalized by the empirical sublimation radii vs total luminosity. The emitting radius is measured from the HWHM of the emission lines. Markers/colors are the same as in Figure 4. $\beta = 0.42_{-0.23}^{+0.62}$, $\rho = 0.54_{-0.31}^{+0.75}$, $\sigma = 0.64_{-0.50}^{+0.78}$.

Table 2. Median and HDI for the slope, correlation coefficient, and intrinsic scatter for each the linear regression fits of CO emitting radii.

Relation	Type	β	ρ	σ
R_{CO} vs L_*	Winds	$0.47_{-0.29}^{+0.28}$	$0.59_{-0.33}^{+0.26}$	$0.48_{-0.14}^{+0.16}$
	Disk	$-0.45_{-0.52}^{+0.40}$	$-0.52_{-0.47}^{+0.45}$	$0.64_{-0.24}^{+0.35}$
R_{CO}/R_{sub} vs L_*	Winds	$0.26_{-0.39}^{+0.26}$	$0.38_{-0.39}^{+0.36}$	$0.47_{-0.13}^{+0.16}$
	Disk	$-0.75_{-0.49}^{+0.51}$	$-0.71_{-0.29}^{+0.35}$	$0.64_{-0.26}^{+0.34}$

Revisiting The Inner Rim R_{CO} & R_{sub} Correlation

Salyk et al. (2011) found CO inner radii shows a dependence on dust sublimation and dust shielding from radiation. Salyk et al (2011) calculated the CO inner radius from $1.7 \times$ HWHM Keplerian velocities in their survey. They found the CO inner radius moves to larger radii in more luminous stars in different types of disks and follow a similar but steeper trend to the dust sublimation temperatures of $T \sim 1500-2000$ K. In this work we revisit this previous finding with new spectra and increase the sample size going from 32 young stars with circumstellar disks to 51 objects. The original sample spans more than two orders of magnitude in stellar+accretion luminosity, and now our dataset spans about

four orders of magnitude in luminosities, as shown in Figure 8-9. Following Salyk et al. (2011), objects are sub-divided as follows: T-Tauri have effective temperatures lower than 7000 K, HAeBe have temperatures higher than 7000 K, and Transitional disks have infrared index above 0.8. As in Salyk et al. (2011), we draw dust sublimation radii lines to compare the CO radii to dust radii and assume blackbody grains in a disk with optically thin inner region, where the dust sublimation radius scales as

$$T_{sub} \approx \left(\frac{L_*}{16\sigma\pi R_{sub}^2} \right)^{1/4}. \quad 2$$

Similarly to Salyk et al. (2011), we find a positive trend between CO emitting inner radius reminiscent of the dust sublimation relation at temperatures of $\sim 1000 - 2000\text{K}$ shown in Figure 10. Transitional disk CO radii are larger than their TTs and HAeBe counterparts, similarly to what found in Salyk et al. (2011). These results suggest the CO inner radius moves outward for hotter stars similar to the dust sublimation radius, and dust cavities correlate with larger CO emitting radii. In addition, on the right side of Figure 10 we distinguish the kinematics of the gas by the emission shapes and learn that the double-peak subset follows a tentative negative trend. For systems with total luminosity between 10 and $10^3 L_{\odot}$ and Keplerian emission, the observed CO inner radius slowly moves inward as opposed to both inner dust disk sizes set by dust sublimation and narrow wind-like emission. This discontinuity and opposing behaviour at higher M_* systems suggest a CO source close to the host stars is emitted only at very high temperatures or extreme environments around stellar masses of $\sim 4 M_{\odot}$. This phenomena becomes more evident when normalizing each R_{CO} with their respective R_{sub} as in Figure 11. The relationship between R_{CO}/R_{sub} for the subset of high luminosity HAeBe stars follows a downward trend. A possible explanation to this phenomena is discussed in the

next section.

As for the wind broad components, we see large scatter at low stellar luminosities and a trend indicating a similar behaviour to the dust sublimation radius, $R_{sub} \propto \sqrt{L_*}$ as seen in Figure 10. Once normalized by the dust sublimation radii for each system we find the wind broad component emitting radii have large scatter with no clear trend. An apparent slow positive trend can be seen and attributed to the Transitional disks around TTs with emitting regions at larger radii. The scatter of the TTs subset is around a median of $R_{inner\ CO}/R_{sub} = 1$. These points suggest that TTs wind broad components seem to move with the dust sublimation radius and is proportional to the square root of the total luminosity or slightly steeper, similar to what Salyk et al. (2011) found.

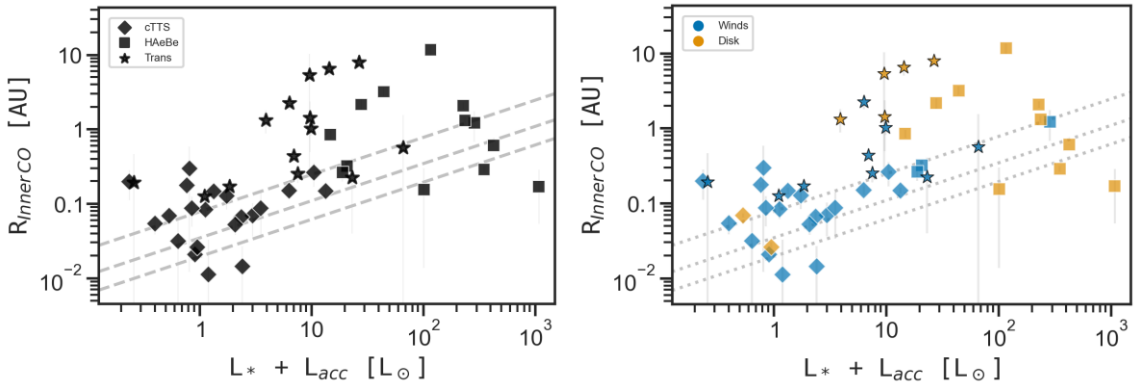


Figure 10. CO emitting radii measured from the width of emission line base (10%) that traces the fastest CO and closest to the star. The x-axis is the total luminosity as seen from the disk, the composite stellar and accretion luminosities. The dashed lines show theoretical curves for dust sublimation radius as a function of luminosity like Salyk et al (2011). The CO emitting radii uncertainties are shown and are significant for disks of low inclination. IQ Tau – a low luminosity object with Keplerian emission – is missing due to lack of L_{acc} measurement.

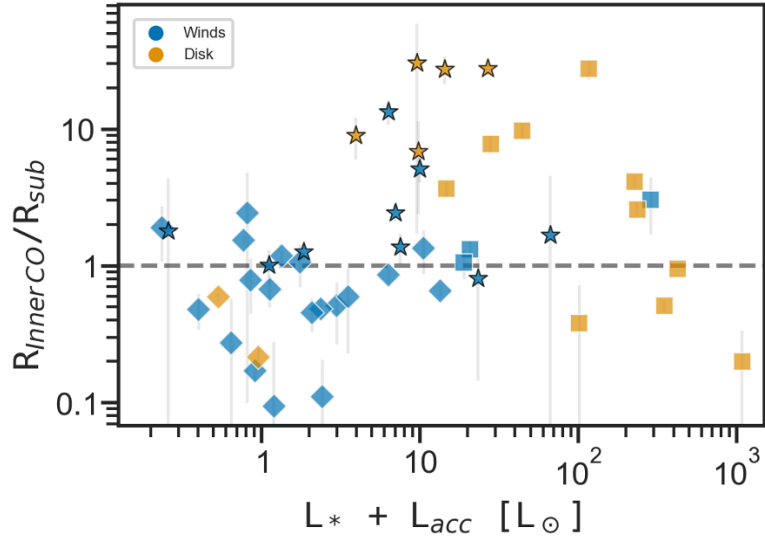


Figure 11. CO emitting radii of innermost CO normalized by the empirical sublimation radii of each system vs the total luminosity. Symbols are the same as in Figure 4 and 5. The horizontal dashed line highlights $R_{CO}/R_{sub} = 1$.

Discussion of Keplerian Emitting Regions

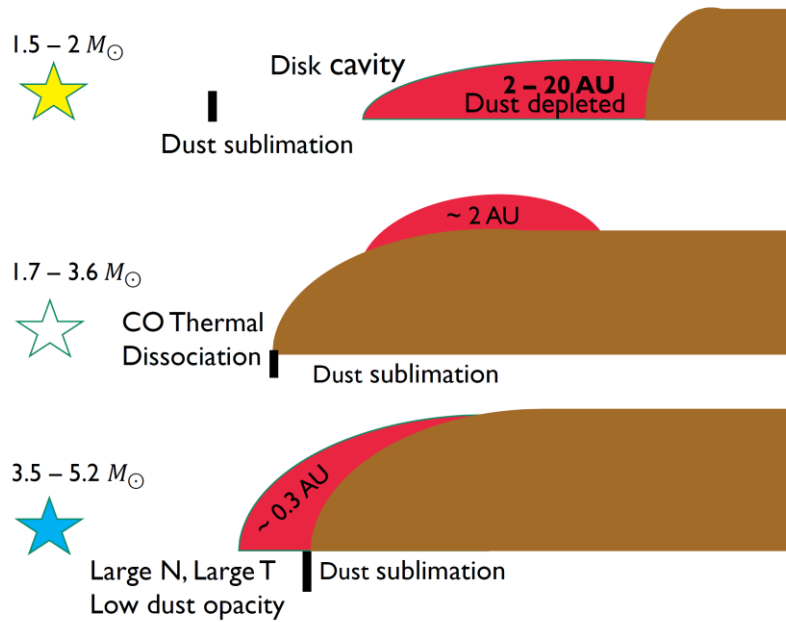


Figure 12. Schematic of three main Keplerian emission regions. The stellar masses of each category are listed on the left side, and a disk cross section is drawn on the right side. The red part of the disk is the CO emitting region, and the brown is the dust optically thick region.

The multiple parameters of some of these systems can be summarized using schematics of cross sections of protoplanetary disks and drawing the CO emitting regions. The main emitting regions are categorized in Figure 12 by stellar mass, and the correlated total luminosity. This is chosen because several properties seem to correlate with this parameter as we will see. The left side of the schematic shows the stellar masses that separate these types of systems. The dust sublimation radius is drawn and as expected increases for more massive and hotter stars.

The lower mass Herbig Ae/Be systems (top of Figure 12) show inner dust depletion traced by their $n_{1330} > 0$, as seen in Figure 4. The host stars of these disks have a stellar luminosity of $4 - 27 L_{\odot}$ and effective temperatures of $5,500 - 9,750\text{K}$. Approximate inner dust cavity sizes from spatially-resolved millimeter interferometry show some emission lie close to the cavity wall such as HD169142 ($R_{cav} \sim R_{CO}$), while others lie well within the cavity like SR21 ($R_{cav} \sim 25 R_{CO}$) (Andrea Banzatti et al., 2022). These systems show the Keplerian emission at the largest distances from the central star, up to 20 AU. Furthermore, the absence of high velocity gas at closer distances is interpreted as a cavity of CO gas. Therefore, CO emission is located or trapped between the molecular cavity and the disk cavity. The observed low CO luminosities are likely caused not only by the colder and distant gas but also the smaller emission areas limited to the ring between the gas and dust cavities. A similar scenario of a CO emitting layer between a gas and dust cavity is discussed in Bosman et al. (2019). They suggest this is not caused by photodissociation but attribute it to a drop in gas or column densities of gas closer to the star, they suggest it may trace giant planets carving an inner disk hole, and indicate other mechanisms do not create systems with different

cavity sizes in dust and gas.

The second part of the schematic show systems of higher mass Herbig stars of luminosity $14 - 230 L_{\odot}$ and effective temperature $7,250 - 11,500$ K with VVser reaching up to $14,000$ K. These disks have infrared index < 0 , tracing fuller inner dust regions without cavities so the dust disk is likely to reach the dust sublimation radius. These disks show CO emission from $4 - 10 R_{sub}$, suggesting a surface layer of CO above the optically thick midplane located at $1.4 - 3.5$ AU from the star. The inner R_{CO} measurements from the line wings show no CO emission within the sublimation radius indicating no CO at the inner rim. Bosman et al. 2019 discusses a similar scenario for CO emission at $R_{CO} < 5$ AU consistent with the emission in this category. Their models show gas temperatures might be high enough (>3000 K) to keep gas atomic and dissociate CO near the dust sublimation radius, and the gas cools down and can become molecular at larger radii above the dust IR photosphere. The CO emission in this region has lower column densities and gas-to-dust ratio than the dust depleted regions from the previous category. Yet, the CO luminosity range of this category is brighter. This is likely due to the higher gas temperatures coupled with the dust surface at this closer distances to more massive stars, and the potential for larger covered emission areas in contrast to the colder trapped gas.

The last category in the schematic consists of massive HAeBe stars of stellar luminosity up to $1000 L_{\odot}$ and effective temperature of $7,250$ K up to $12,500$ K. The Keplerian emission lines of these disks are the broadest in our dataset, and show CO emission very close to the star down to fractions of AU within the sublimation radius – which has moved from ~ 0.1 AU up to ~ 0.6 AU as shown in Figure 4. The disks for these

massive stars may be larger in mass – as suggested by steep disk mass to stellar mass relations (e.g., Pascucci et al., 2016). As the dust slowly recedes further back for higher mass stars due to dust sublimation, high column densities of CO are potentially left exposed to the radiation of the host star. While Bosman et al. 2019 do not focus on these innermost regions, they discuss that at high densities ($10^{12} - 10^{14} \text{ cm}^{-3}$) CO production rate may be faster than CO dissociation from the UV radiation field expected at the sublimation radius, and gas temperatures can increase far above the dust temperatures. The thermo-chemical model they use for the inner disk estimates a slower molecular to atomic transition at even higher temperatures than equilibrium models. While they note the modeled CO abundances may be overestimated, we do in fact observe this emission area. In the data we observe gas closest to the dust-free region at or near dust sublimation have higher CO luminosity than CO emissions at farther radii. Bosman et al. (2019) mentions that their model's inner rim region produces $\sim 40\%$ of the $v=1-0$ flux – which is removed in their work due to the focus on small inner cavities. These emission areas likely dominate the CO luminosity due to the expected high column densities of CO or very high gas temperatures. This case is specially interesting because this emission area challenges our knowledge on the thermo-chemical limits of CO dissociation in these extreme environments.

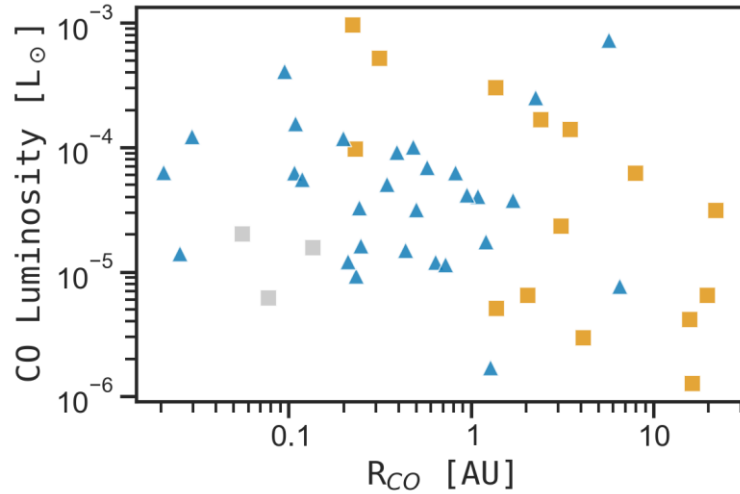


Figure 13. CO luminosity (BC/SC) as a function of CO characteristic emitting radii. These two measurements correlate with stellar mass and luminosity. The markers/colors are the same as in Figure 4 and 5.

Molecular Wind in Transitional Disks

Transitional disks set interesting environments where CO in both Keplerian and Wind-like motion survives within the cavities of these systems. We discussed the former case in the last section, but the later is an interesting case because these molecular winds may be related to the physical processes that produce the disk cavities.

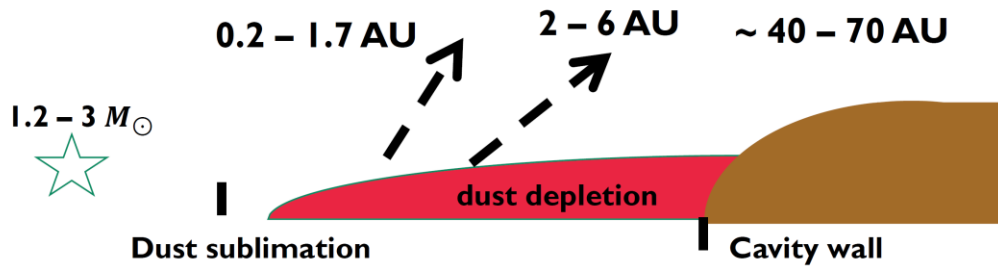


Figure 14. Schematic of molecular winds within dust depletion regions. It follows the similar format as Figure 12. Molecular wind radii are marked by the arrows. For these systems dust sublimation is down to about 0.1 AU.

We observe BC of triangular emission that trace CO emission at radii of 0.2 – 6 AU within cavities that have been measured from near-infrared interferometry of at least

40 AU. This emission region is in 6 cTTs (DoAr44, HD135344B, LkHa330, RY Lup, SUAur, TW Hya) and 2 HAeBe (ABAur, MWC758) with masses of $1.2 - 3M_{\odot}$. Similar to the first case discussed in the last section, CO is found within dust cavities. Only, in this case we find it much closer to the central star. This is likely due to the lower molecular gas temperatures at lower mass systems, and lower CO photo-dissociation due to UV dominated radiation fields in HAeBe. In fact, ABAur and MWC758 have larger R_{CO} than their cTTs counterparts in this scenario; with exception of HD135344B whose inner emitting region is unusually pushed out to 6 AU and shows the most depleted region in this subset.

The innermost component of the CO molecular emission traces regions that are complex and have multiple contributions to outflowing gas from star such as accretion-powered stellar winds, magneto-hydrodynamic (MHD) winds caused by stellar field lines and disk interactions, and failed winds (Ilaria Pascucci et al., 2022). Most of these processes launch gas outflows with velocities beyond 100 km/s, and others create onion-shaped structures with a velocity gradients like magnetocentrifugal winds (MCW) that can be triggered over a range of disk radii. Since the BC we measure in this subset indicate velocities of < 100 km/s it is possible these regions are the lower velocity layers of the launching regions of MCW. The cavities in these disks create environments with low surface density that can result in magnetorotational instability (MRI) active regions that are known to enhance disk wind uplift, similar to MRI-active regions due to low column densities in the outer disk (Pascucci et al., 2022). More work needs to be done in exploring the launching mechanisms in these regions to learn which regions and which type of winds the CO spectra may trace. The fact that the molecule CO may trace part of

an inner disk wind is very important to understand the physical, irradiation, and in turn the chemical conditions of inner disk winds, all of which are still largely unknown.

Low Mass Disks

There are three low mass TTs that trigger CO in Keplerian emission near or at the sublimation radius: IQ Tau, WaOph6, AA Tau. The temperatures of these disks should be lower than their counterparts around stars of higher mass. In addition, weaker UV radiation fields capable of photo-dissociating CO should be less common and possible at smaller radii than the higher stellar mass objects. We saw this effect in Figures 8-10 where the CO emitting region generally moves outward for disks around higher L_* stars. These low mass objects don't have significant cavities – traced from the infrared index – which increases CO survivability from photo-dissociation at smaller radii due to dust shielding as seen in the second case in Figure 12. However, the lack of a slow moving component in these three systems is intriguing as all other systems have it instead, as seen in Figure 4. While these systems seem to follow general expectations, the observed Keplerian profile is what motivates us to count them as partial outliers, especially in the CO luminosity analysis. More work needs to be done to look into why it is we observe Keplerian profiles in this regime of the dataset.

Outliers

MWC 297 is a very bright system and AllWise only has upper limit measurements and measured a 0.7 SNR for the W2 photometric measurement with up to 32% of the pixels affected by saturation. This system is considerably higher in stellar mass, luminosity and effective temperature. The measured single-component Keplerian line is often an outlier in the studied trends. Therefore we choose to exclude it in all

analysis.

TW Hya is the system with the lowest stellar mass in the sample and it is the dimmest in terms of CO luminosity. It is a strong outlier in the inclination and stellar mass parameter among the cTTs and wind emission systems, so we chose to exclude it from all analysis

IV. CONCLUSIONS

In this work, we used observations of CO emission for a sample of ~ 51 cTTs, HAeBe, and transitional disks to probe CO molecular gas emission regions in inner disks at < 10 au. We classified each protoplanetary system by their kinematic line shapes as double-peaked lines (interpreted as gas in Keplerian rotation around the star) vs triangular lines (interpreted as including wind emission at sub-Keplerian velocity filling in the line center). Using this classification, we study the differences between these two subsets along with their excitation, stellar and disk parameters.

Building on recent work, in this study we focus on CO excitation by using the measured luminosities of CO $v = 1-0$ fundamental lines. We find that CO luminosity in double-peaked lines correlates strongly with both stellar mass/luminosity and inclination, while triangular lines exhibit a large scatter and no correlation as a function of stellar mass but shows a flat or negative correlation with inclination. A possible interpretation of the Keplerian emission trend is a strong coupling between gas and dust temperatures which can induce temperature and luminosity profiles that increase with the luminosity of the central star that heats up the dust. The triangular emission in contrast shows large scatter and no clear trend, suggesting a weak coupling between gas and dust temperatures or an alternative dominant driver for CO luminosity introduced by the stronger coupling of gas to magnetic field causing the wind in these systems and the wind launching mechanisms.

The CO luminosity also shows clear correlations with inclination. Geometrical effects have long been known to affect measurements such as CO line fluxes and shapes, but they are not well understood, especially in the case of inner disk winds. For Keplerian

emission we assume thick rings of gas with an inner wall edge for most systems. CO near the inner wall of the disk has shown to dominate in a thermo-chemical model (Bosman et al., 2019), and it is suggested by the positive CO luminosity trend with inclination. In connection to that, line widths increase as a function of disk inclinations due to the higher radial velocities observed along the line of sight. If a larger area of the inner disk wall becomes visible at higher inclinations, we should observe an increase in CO luminosity measurements possibly explaining the trend in the data. In disks with wind-type line profiles, instead, an opposing trend appears where CO emission from the triangular wing line components could perhaps be obscured by dusty winds and an increase in material along the line-of-sight for highly inclined systems. This trend is less understood and more uncertain, as the correlation between the CO luminosity and inclination is weak. More work needs to be done to understand how the viewing angle may change the observed properties of different emitting regions.

We also revisited a previous study on the innermost CO emitting radii as a function of total luminosity (accretion+star). As Salyk et al. (2011) found, we observe a general trend of CO moving to larger radii for higher total luminosities. We add that once we separate Keplerian from wind emission, we observe opposing trends of CO where double peak emission moves inward for more massive central stars, and wind emission instead moves outward like the dust sublimation radius. This work helps us understand the different emission regions the line shapes trace and start as foundation for creating schematics of these regions.

In the case of double-peaked lines, find three main Keplerian emission regions

- CO emission within dust depleted regions and inner rim of cavities. This gas is

the lowest in temperature among these emission regions, but requires high column densities and very high gas-to-dust ratios $>10,000$ (Bosman et al., 2019). In addition, these systems show a molecular gas depletion at short distances that indicate separate gas and dust size cavities carved by processes such as planet formation or disk dispersal by winds.

- A molecular surface layer past the dust sublimation radius of warmer molecular gas closer to the star that is triggered at relatively low column densities $<10^{18} \text{ cm}^{-2}$. CO near the sublimation radius is photo-dissociated.
- Inner rim hot molecular gas around the most massive stars. This emission region is only possible due to large densities in these massive systems, and possibly large column densities revealed by the receding dust sublimation radius.

In addition, we discuss a case where the CO broad component in wind-type spectra is found within large cavities. This molecular gas is located between 0.2 – 6 AU within dust cavities that may extend out to ~ 70 AU in some disks. We highlight that the large range of CO radii is likely due to the better survival of CO around colder stars in contrast to HAeBe, specially at smaller radii. In addition, detecting launching regions of winds this close to stars within dust depletion (high gas-to-dust ratio) regions provides important data to study the types of mechanisms that launch these inner disk winds. Scenarios that are currently being investigated include the increase of disk gas uplift due to the low surface density through magnetorotational instability (Pascucci et al., 2022).

Interesting future directions of investigations include fitting the observations using simple disk slab models to estimate best-fit temperature and initial abundance ratios of the CO molecular gas, and full Keplerian line model fits to accurately estimate the

emitting radius of the observed lines. These measurements can be used to constrain detailed thermo-chemical models that are used to simulate the gas and dust transport and help us better understand the composition profile of protoplanetary disks, and therefore planet formation. In addition, further works needs to be done to characterize the launching wind dust depletion emitting region to better constrain the limitations of the current models of these processes such as accretion-powered launched winds or interactions between the inner disk and stellar magnetic field lines.

APPENDIX

Table A1. Sample spectra properties

Name	Comp	Shape	FW10 % (km/s)	FWHM (km/s)	Flux v=1- 0 (erg s ⁻¹ cm ⁻²)	Flux v=1- 0 err (erg s ⁻¹ cm ⁻²)	Instru
AA Tau	SC	DP	166.5	118.3	7.91e-14	5.51e-16	CRIRES
AB Aur	SC	T	24.25	12.14	9.11e-15	1.49e-17	iSHELL
AS205N	NC	T	72.2	14.11	1.99e-14	4.97e-17	iSHELL
AS205N	BC			57.54	4.48e-14	2.49e-16	
CITau	NC	T	266.9	104.7	3.56e-14	6.30e-16	iSHELL
CITau	BC			241.5	2.72e-14	6.30e-16	
CQTau	NC	T	83.5	7.342	8.92e-16	1.55e-17	iSHELL
CQTau	BC			52.36	5.99e-15	1.00e-16	
CV Cha	SC	T	132.95	75.07	4.61e-14	1.39e-16	CRIRES
CW Tau	SC	T	129.3	71.6	7.21e-14	1.31e-16	CRIRES
DF Tau	NC	T	138.65	37.2	1.67e-14	1.22e-16	CRIRES
DF Tau	BC			80.9	4.89e-14	1.22e-16	
DR Tau	NC	T	49.25	10.61	2.11e-14	2.71e-17	CRIRES
DR Tau	BC			30.29	5.39e-14	4.15e-17	
DoAr44	SC	T	98.25	52.72	3.80e-14	1.15e-16	CRIRES
Elias20	NC	T	121.3	49.75	3.94e-14	8.72e-16	iSHELL
Elias20	BC			94.95	6.71e-14	8.72e-16	
FN Tau	SC	T	20.5	9.875	1.03e-14	3.30e-16	CRIRES
FZ Tau	SC	T	60.15	30.11	7.20e-14	3.26e-15	CRIRES
GQ Lup	BC	T	119.8	91.8	2.19e-14	1.15e-16	CRIRES
GQ Lup	NC			65.75	2.47e-14	1.15e-16	
HD1353 44B	BC	T	31.1	18.30	3.83e-15	5.04e-17	CRIRES
HD1353 44B	NC			9.736	2.52e-15	3.56e-17	
HD1415 69	SC	DP	26.35	16.7	2.68e-14	2.34e-16	iSHELL
HD1426 66	SC	DP	70.95	55.7	2.54e-15	1.15e-16	iSHELL
HD1430 06	SC	DP	31.05	25.05	5.26e-15	2.08e-16	iSHELL
HD1501 93	SC	DP	44.7	37.25	5.11e-15	1.34e-16	iSHELL
HD1632 96	SC	T	111.55	60.60	1.10e-14	8.13e-17	iSHELL
HD1691 42	SC	DP	11.85	6.775	3.31e-15	6.66e-17	iSHELL

HD1792 18	SC	DP	24.35	17.75	3.10e-15	1.74e-17	iSHELL
HD1900 73	SC	T	33.6	15.52	5.43e-15	1.25e-17	iSHELL
HD2594 31	NC			59.6	5.06e-15	1.32e-16	
HD2594 31	BC	DP	137.15	119.4	7.90e-15	1.32e-16	iSHELL
HD3592 9	SC	DP	149.6	122.6	1.96e-14	2.20e-16	iSHELL
HD3691 7	SC	DP	159.5	106.7	1.77e-14	2.27e-16	iSHELL
HD3780 6	SC	DP	67.1	51.8	4.24e-15	8.09e-17	iSHELL
HD5864 7	SC	DP	199.25	191.2	1.82e-14	8.27e-17	iSHELL
IQ Tau	SC	DP	190.6	133.6	3.31e-14	1.11e-15	CRIRES
IRS48	SC	DP	22.1	14.2	3.82e-15	1.62e-16	iSHELL
LkHa33 0	NC			10.26	3.38e-15	8.10e-17	
LkHa33 0	BC	T	45	30.05	7.81e-15	1.78e-16	iSHELL
MWC29 7	SC	DP	68.9	46.75	1.86e-14	1.48e-17	iSHELL
MWC48 0	SC	T	94.25	49.48	1.20e-14	6.79e-17	iSHELL
MWC75 8	BC			37.64	1.03e-14	6.49e-17	
MWC75 8	NC	T	48.35	11.59	7.61e-15	2.18e-17	iSHELL
RNO90	NC	T	150.75	54.25	3.61e-14	1.11e-16	iSHELL
RNO90	BC			83.95	6.14e-14	1.11e-16	
RU Lup	NC	T	101.65	19.95	2.61e-14	9.73e-17	CRIRES
RU Lup	BC			84.72	4.70e-14	1.01e-16	
RY Lup	NC	T	130.35	18.16	1.10e-14	7.26e-17	CRIRES
RY Lup	BC			110.7	8.80e-15	8.90e-17	
RYTau	NC	T	200.8	54.26	6.10e-15	1.35e-16	iSHELL
RYTau	BC			125.7	1.10e-14	1.40e-16	
S CrA N	NC	T	63.5	9.313	9.88e-15	1.12e-17	CRIRES
S CrA N	BC			36.13	3.04e-14	7.57e-17	
SR21	SC	DP	17.3	10.15	4.59e-15	1.07e-16	iSHELL
SUAur	SC	T	100.5	60.66	8.06e-15	1.12e-16	iSHELL
SX Cha	SC	T	81.75	42.67	2.09e-14	7.78e-16	CRIRES
TW Cha	SC	T	132.1	66.69	6.55e-14	1.22e-15	CRIRES
TW Hya	SC	T	12.95	7.344	2.19e-14	5.48e-17	CRIRES

V892Tau	SC	DP	45.45	28.8	3.72e-14	3.09e-17	iSHELL
VV CrA	NC			18.75	9.70e-15	2.35e-17	
S		T					CRIRES
VV CrA	BC		102.4	75.95	1.70e-14	4.13e-17	
S							
VV Ser	SC	DP	84.45	62.25	8.72e-15	1.02e-16	iSHELL
VW Cha	BC			71.79	8.18e-14	2.20e-16	
VW Cha	NC	T	108.85	25.15	3.21e-14	2.08e-16	CRIRES
VZ Cha	SC	T	82.9	42.63	1.10e-13	6.22e-16	CRIRES
WX Cha	NC			67.95	3.01e-14	1.18e-15	
WX Cha	BC	T	165.9	131.8	5.52e-14	1.18e-15	CRIRES
WaOph	SC	DP	215.6	147.45	4.20e-14	1.47e-16	CRIRES
6							

Notes: T stands for Triangular shape and DP is double-peak shape. Comp=Component; Instru=Instrument source of spectra.

Sources: (Banzatti & Pontoppidan, 2015; Andrea Banzatti et al., 2022; Brown et al., 2013; Pontoppidan et al., 2011)

Table A2. Sample stellar and disk properties

Name	Dist (pc)	T_{eff} (K)	M_* (M_\odot)	L_* (L_\odot)	$\log L_{acc} / L_\odot$	n_{13-3}	Incl (deg)	F_{W2} (Jy)	R_{sub} (AU)
AA Tau	136.7	3800	0.6	0.50	-1.43	- 0.34	71	0.34	0.116
AB Aur	155.0	9000	2.36	45.7 1	1.32	0.81	11.5	36.69	0.340
AS205	127.5	4210	0.87	2.14	-0.07	- 0.19	20	6.81	0.136
N									
CITau	158.0	4150	0.71	0.78	-0.87	- 0.16	50	0.66	0.122
CQTau	148.6	6750	1.5	6.61	-0.03	0.78	35	2.89	0.183
CV Cha	192.2	5180	2.1	8.00	0.41	- 0.23	52	1.18	0.195
CW Tau	131.9	4540	1.01	0.45	-0.49	- 0.72	65	1.76	0.115
DF Tau	124.5	3450	0.6	0.90	-0.63	- 1.09	60	1.38	0.124
DoAr44	145.3	4540	1.22	0.93	-0.73	0.81	32	0.59	0.124
DR Tau	194.6	4100	0.93	0.63	-0.24	- 0.34	5.2	1.91	0.119
Elias20	138.1	3900	0.48	2.24	-0.87	- 0.34	49		0.137
FN Tau	130.8	3300	0.3	0.80	-1.77	- 0.04	20		0.122

FZ Tau	129.6	3800	0.63	0.32	-0.27	- 0.93	22	1.34	0.111
GQ Lup	151.2	4210	0.78	0.91	-0.36	- 0.19	60.5	1.03	0.124
HD1353 44B	134.4	6250	1.46	5.13	0.09	1.88	40.5	3.54	0.168
HD1415 69	111.1	9750	2.12	25.1 2	0.22	1.30	58.5	0.62	0.286
HD1426 66	145.5	7250	1.75	13.4 9	0.12	- 0.49	55.9	3.04	0.233
HD1430 06	166.4	5500	1.74	3.47	-0.32	1.25	27.1	1.42	0.148
HD1501 93	150.0	9000	2.25	22.9 1	0.71	- 0.48	47.2	6.48	0.277
HD1632 96	100.6	8750	1.91	15.4 9	0.73	- 0.50	50.2	11.61	0.243
HD1691 42	114.4	7250	1.55	5.75	0.59	1.47	21.6	0.94	0.175
HD1792 18	258.0	9750	2.99	104. 7	1.08	0.13	53.8	4.82	0.424
HD1900 73	872.4	9230	2.85	83.2 0	2.31	- 1.28	21.6	5.63	0.399
HD2594 31	640.0	1250 0	5.24	813	2.43	0.55	24.5	9.55	0.852
HD3592 9	376.7	7250	3.53	93.3 3	0.91	- 1.96	31.8	1.11	0.412
HD3691 7	445.0	1150 0	4.36	407. 38	1.28	- 0.18	89.4	2.74	0.639
HD3780 6	397.1	1075 0	3.52	199. 53	1.46	- 1.14	60	6.66	0.505
HD5864 7	302.2	1075 0	4.05	309. 03	1.62	- 1.91	63.3	10.04	0.570
IQ Tau	130.8	3700	0.5	0.71		- 0.37	62.1		0.121
IRS48	125.0	9000	2	14.3 0	-0.89	1.33	42		0.237
LkHa33 0	308.4	6300	2.95	22.9 0	-0.46	1.90	12	1.36	0.277
MWC2 97	407.8	2600 0	19.98	6025 6	4.08		27.1	951	2.678
MWC4 80	155.2	8000	1.85	16.6 0	0.39	- 0.79	36.5	4.59	0.249
MWC7 58	155.0	7250	1.64	8.71	0.1	0.82	40	4.85	0.201
RNO90	116.6	5660	1.5	5.70	-0.19	- 0.52	53	3.86	0.174

RU Lup	158.9	4020	0.55	1.45	-0.01	-	16	1.70	0.130
RY Lup	158.4	4900	1.27	1.82	-1.4	0.54	53	1.34	0.134
RYTau	443.7	5930	2.04	12.3	0.07	-	65		0.225
S CrA				0		0.19			
N	152.3	4000	0.7	0.66	0.04	-	27		0.120
SR21	137.9	6300	1.79	9.55	-0.7	0.09	15	1.08	0.207
SUAur	157.7	5500	2.07	6.20	-0.1	2.01	51	2.79	0.179
SX Cha	184.0	4060	0.77	0.18	-1.25	-	44		0.104
						0.47			
TW Cha	184.2	4060	1	0.38	-1.66	-	31		0.113
						0.14			
TW Hya	60.0	3800	0.61	0.23	-1.53	0.96	7	0.30	0.107
V892Ta						-			
u	117.1	1150	2.8	40.0	0.65	-	54.5		0.328
		0		0		0.13			
VV CrA	148.8	3700	0.55	0.47	0.21	0.04	32	34.68	0.115
S									
VVSer	403.4	1400	3.61	204.	1.51	-	58.7	3.75	0.508
		0		17		1.24			
VW	190.0	4200	0.6	3.37	-0.77	-	44	1.28	0.146
Cha						0.12			
VZ Cha	191.2	4000	0.8	0.46	-0.73	-	16	0.44	0.115
						1.07			
WaOph	123.4	4200	0.63	0.74	-0.66	-	47.3	1.00	0.121
6						0.39			
WX	190.0	3670	0.5	0.84		-		0.43	0.123
Cha						1.02			

Sources: (Andrews et al., 2018; Bailer-Jones et al., 2018; Banzatti & Pontoppidan, 2015; Fang et al., 2018; Guzmán-Díaz et al., 2021; Herczeg & Hillenbrand, 2014; Huang et al., 2018; Kurtovic et al., 2018; Lazareff et al., 2017; Perraut et al., 2019; Pinilla et al., 2018; Salyk et al., 2013; Ubeira Gabellini et al., 2019; Cutri et al. 2021)

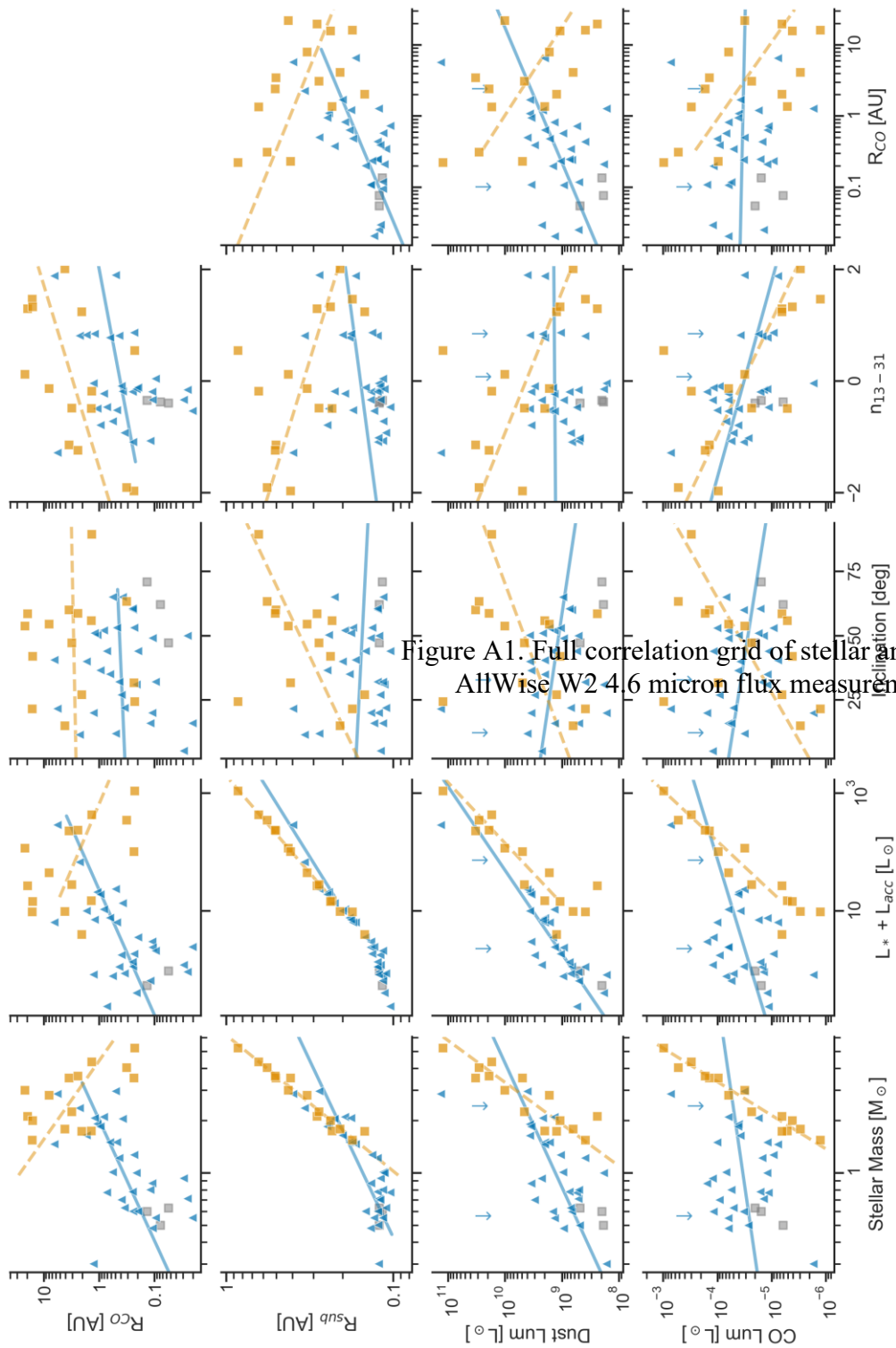


Figure A1. Full correlation grid of stellar and disk parameters of the sample. The parameters shown are: Stellar Mass [M_{\odot}], $L_* + L_{\text{acc}}$ [L_{\odot}], Inclination [deg], n_{13-31} , and R_{co} [AU]. The diagonal plots show the distribution of each parameter. The off-diagonal plots show the correlation between pairs of parameters. The data points are color-coded: blue triangles, orange squares, and grey squares. Solid blue lines and dashed orange lines represent different correlation models. Blue arrows pointing downwards indicate upper limits.

REFERENCES

- Andrews, S. M., Huang, J., Pérez, L. M., Isella, A., Dullemond, C. P., Kurtovic, N. T., Guzmán, V. V., Carpenter, J. M., Wilner, D. J., Zhang, S., Zhu, Z., Birnstiel, T., Bai, X.-N., Benisty, M., Meredith Hughes, A., Öberg, K. I., & Ricci, L. (2018). The Disk Substructures at High Angular Resolution Project (DSHARP). I. Motivation, Sample, Calibration, and Overview. *The Astrophysical Journal Letters*, 869(2), L41.
- Armitage, P. J. (2010). Dynamics of Protoplanetary Disks. In *arXiv [astro-ph.SR]*. arXiv. <http://arxiv.org/abs/1011.1496>
- Bailer-Jones, C. A. L., Rybizki, J., Fouesneau, M., Mantelet, G., & Andrae, R. (2018). Estimating Distance from Parallaxes. IV. Distances to 1.33 Billion Stars in Gaia Data Release 2. *AJS; American Journal of Sociology*, 156(2), 58.
- Banzatti, A., & Pontoppidan, K. M. (2015). AN EMPIRICAL SEQUENCE OF DISK GAP OPENING REVEALED BY ROVIBRATIONAL CO. *The Astrophysical Journal*, 809(2), 167.
- Banzatti, Andrea, Abernathy, K. M., Brittain, S., Bosman, A. D., Pontoppidan, K. M., Boogert, A., Jensen, S., Carr, J., Najita, J., Grant, S., Sigler, R. M., Sanchez, M. A., Kern, J., & Rayner, J. T. (2022). Scanning disk rings and winds in CO at 0.01-10 au: a high-resolution M-band spectroscopy survey with IRTF-iSHELL. In *arXiv [astro-ph.SR]*. arXiv. <http://arxiv.org/abs/2202.03438>
- Banzatti, Andrea, Pascucci, I., Edwards, S., Fang, M., Gorti, U., & Flock, M. (2019). Kinematic Links and the Coevolution of MHD Winds, Jets, and Inner Disks from a High-resolution Optical [] Survey. *The Astrophysical Journal*, 870(2), 76.
- Bast, J. E., Brown, J. M., Herczeg, G. J., van Dishoeck, E. F., & Pontoppidan, K. M. (2011). Single peaked CO emission line profiles from the inner regions of protoplanetary disks. *Astronomy & Astrophysics. Supplement Series*, 527, A119.
- Bosman, A. D., Banzatti, A., Bruderer, S., Tielens, A. G. G., Blake, G. A., & van Dishoeck, E. F. (2019). Probing planet formation and disk substructures in the inner disk of Herbig Ae stars with CO rovibrational emission. *Astronomy & Astrophysics. Supplement Series*, 631, A133.
- Brown, J. M., Blake, G. A., Dullemond, C. P., Merín, B., Augereau, J. C., Boogert, A. C. A., Evans, N. J., II, Geers, V. C., Lahuis, F., Kessler-Silacci, J. E., Pontoppidan, K. M., & van Dishoeck, E. F. (2007). Cold Disks: Spitzer Spectroscopy of Disks around Young Stars with Large Gaps. *The Astrophysical Journal*, 664(2), L107.

- Brown, J. M., Pontoppidan, K. M., van Dishoeck, E. F., Herczeg, G. J., Blake, G. A., & Smette, A. (2013). VLT-CRIRES Survey of Rovibrational CO Emission from Protoplanetary Disks. *The Astrophysical Journal*, 770, 94.
- Espaillet, C., Muzerolle, J., Najita, J., Andrews, S., Zhu, Z., Calvet, N., Kraus, S., Hashimoto, J., Kraus, A., & D'Alessio, P. (2014). An Observational Perspective of Transitional Disks. In *arXiv [astro-ph.SR]*. arXiv. <http://arxiv.org/abs/1402.7103>
- Fang, M., Pascucci, I., Edwards, S., Gorti, U., Banzatti, A., Flock, M., Hartigan, P., Herczeg, G. J., & Dupree, A. K. (2018). A New Look at T Tauri Star Forbidden Lines: MHD-driven Winds from the Inner Disk. *The Astrophysical Journal*, 868, 28.
- Furlan, E., Hartmann, L., Calvet, N., D'Alessio, P., Franco-Hernández, R., Forrest, W. J., Watson, D. M., Uchida, K. I., Sargent, B., Green, J. D., Keller, L. D., & Herter, T. L. (2006). A Survey and Analysis of Spitzer Infrared Spectrograph Spectra of T Tauri Stars in Taurus. *The Astrophysical Journal Supplement Series*, 165(2), 568.
- Furlan, E., Luhman, K. L., Espaillat, C., D'Alessio, P., Adame, L., Manoj, P., Kim, K. H., Watson, D. M., Forrest, W. J., McClure, M. K., Calvet, N., Sargent, B. A., Green, J. D., & Fischer, W. J. (2011). THE SPITZER INFRARED SPECTROGRAPH SURVEY OF T TAURI STARS IN TAURUS. *The Astrophysical Journal Supplement Series*, 195(1), 3.
- Furlan, E., Watson, D. M., McClure, M. K., Manoj, P., Espaillat, C., D'Alessio, P., Calvet, N., Kim, K. H., Sargent, B. A., Forrest, W. J., & Hartmann, L. (2009). Disk Evolution in the Three Nearby Star-forming Regions of Taurus, Chamaeleon, and Ophiuchus. *The Astrophysical Journal*, 703, 1964–1983.
- Guzmán-Díaz, J., Mendigutía, I., Montesinos, B., Oudmaijer, R. D., Vioque, M., Rodrigo, C., Solano, E., Meeus, G., & Marcos-Arenal, P. (2021). Homogeneous study of Herbig Ae/Be stars from spectral energy distributions and Gaia EDR3. *Astronomy & Astrophysics. Supplement Series*, 650, A182.
- Herczeg, G. J., & Hillenbrand, L. A. (2014). AN OPTICAL SPECTROSCOPIC STUDY OF T TAURI STARS. I. PHOTOSPHERIC PROPERTIES. *The Astrophysical Journal*, 786(2), 97.
- Huang, J., Andrews, S. M., Dullemond, C. P., Isella, A., Pérez, L. M., Guzmán, V. V., Öberg, K. I., Zhu, Z., Zhang, S., Bai, X.-N., Benisty, M., Birnstiel, T., Carpenter, J. M., Meredith Hughes, A., Ricci, L., Weaver, E., & Wilner, D. J. (2018). The Disk Substructures at High Angular Resolution Project (DSHARP). II. Characteristics of Annular Substructures. *The Astrophysical Journal Letters*, 869(2), L42.

- Kurtovic, N. T., Pérez, L. M., Benisty, M., Zhu, Z., Zhang, S., Huang, J., Andrews, S. M., Dullemond, C. P., Isella, A., Bai, X.-N., Carpenter, J. M., Guzmán, V. V., Ricci, L., & Wilner, D. J. (2018). The Disk Substructures at High Angular Resolution Project (DSHARP). IV. Characterizing Substructures and Interactions in Disks around Multiple Star Systems. *The Astrophysical Journal Letters*, 869(2), L44.
- Lazareff, B., Berger, J.-P., Kluska, J., Le Bouquin, J.-B., Benisty, M., Malbet, F., Koen, C., Pinte, C., Thi, W.-F., Absil, O., Baron, F., Delboulbé, A., Duvert, G., Isella, A., Jocu, L., Juhasz, A., Kraus, S., Lachaume, R., Ménard, F., ... Zins, G. (2017). Structure of Herbig Ae/Be disks at the milliarcsecond scale - A statistical survey in the H band using PIONIER-VLTI. *Astronomy & Astrophysics. Supplement Series*, 599, A85.
- Pascucci, I., Testi, L., Herczeg, G. J., Long, F., Manara, C. F., Hendler, N., Mulders, G. D., Krijt, S., Ciesla, F., Henning, T., Mohanty, S., Drabek-Maunder, E., Apai, D., Szűcs, L., Sacco, G., & Olofsson, J. (2016). A Steeper than Linear Disk Mass-Stellar Mass Scaling Relation. *The Astrophysical Journal*, 831(2), 125.
- Pascucci, Ilaria, Cabrit, S., Edwards, S., Gorti, U., Gressel, O., & Suzuki, T. (2022). The Role of Disk Winds in the Evolution and Dispersal of Protoplanetary Disks. In *arXiv [astro-ph.EP]*. arXiv. <http://arxiv.org/abs/2203.10068>
- Perraut, K., Labadie, L., Lazareff, B., Klarman, L., Segura-Cox, D., Benisty, M., Bouvier, J., Brandner, W., Caratti o Garatti, A., Caselli, P., Dougados, C., Garcia, P., Garcia-Lopez, R., Kendrew, S., Koutoulaki, M., Kervella, P., Lin, C.-C., Pineda, J., Sanchez-Bermudez, J., ... Yazici, S. (2019). The GRAVITY Young Stellar Object survey - I. Probing the disks of Herbig Ae/Be stars in terrestrial orbits. *Astronomy & Astrophysics. Supplement Series*, 632, A53.
- Pinilla, P., Tazzari, M., Pascucci, I., Youdin, A. N., Garufi, A., Manara, C. F., Testi, L., van der Plas, G., Barenfeld, S. A., Canovas, H., Cox, E. G., Hendler, N. P., Pérez, L. M., & van der Marel, N. (2018). Homogeneous Analysis of the Dust Morphology of Transition Disks Observed with ALMA: Investigating Dust Trapping and the Origin of the Cavities. *The Astrophysical Journal*, 859(1), 32.
- Pontoppidan, K. M., Blake, G. A., & Smette, A. (2011). The Structure and Dynamics of Molecular Gas in Planet-forming Zones: A CRIRES Spectro-astrometric Survey. *The Astrophysical Journal*, 733, 84.
- Salyk, C., Blake, G. A., Boogert, A. C. A., & Brown, J. M. (2011). CO ROVIBRATIONAL EMISSION AS A PROBE OF INNER DISK STRUCTURE. *The Astrophysical Journal*, 743(2), 112.
- Salyk, Colette, Herczeg, G. J., Brown, J. M., Blake, G. A., Pontoppidan, K. M., & van Dishoeck, E. F. (2013). MEASURING PROTOPLANETARY DISK ACCRETION WITH H i PFUND β . *The Astrophysical Journal*, 769(1), 21.

Ubeira Gabellini, M. G., Miotello, A., Facchini, S., Ragusa, E., Lodato, G., Testi, L., Benisty, M., Bruderer, S., T. Kurtovic, N., Andrews, S., Carpenter, J., Corder, S. A., Dipierro, G., Ercolano, B., Fedele, D., Guidi, G., Henning, T., Isella, A., Kwon, W., ... Wilner, D. (2019). A dust and gas cavity in the disc around CQ Tau revealed by ALMA. *Monthly Notices of the Royal Astronomical Society*, 486(4), 4638–4654.